JOURNAL OF THEORETICAL AND APPLIED MECHANICS
61, 2, pp. 275-287, Warsaw 2023
https://doi.org/10.15632/jtam-pl/162128

ON VISCOELASTIC FIBER JET FORMATION BY FORCESPINNING AT HIGH ROTATION RATE

Daniel N. Riahi

Department of Mechanical Science and Engineering, University of Illinois at Urbana-Champaign, Urbana, IL, USA, and School of Mathematical and Statistical Sciences, University of Texas Rio Grande Valley, Brownsville, Texas, USA

Saulo Orizaga

Department of Mathematics, New Mexico Institute of Mining and Technology, Socorro, New Mexico, USA

e-mail: saulo.orizaga@nmt.edu

We consider a nonlinear three-dimensional viscoelastic fiber jet that is generated during a forcespinning process. We provide a particular case for such a rotating jet at a high rotation rate. We use a viscoelastic constitutive model for the jet equations and then applying a new slender body approach, we continue with proper scaling and perturbation technique to develop a new model for such a jet system. We find that the profiles for jet quantities versus arc length are notably different from all those in related studies reported before for either high or low rotation rates. In particular, jet radius first rapidly decreases as the arc length decreases and then reaches its macro- or nano-scale size not far away from its exit section. The present model can predict a nano-fiber jet that is entirely based on proper scaling, perturbation technique and full fluid mechanics laws and equations.

Keywords: rotating flow, rotating jet, gravity effect, high rotating jet, polymeric fluid

1. Introduction

In a forcespinning process the fluid is driven through an orifice located in a spinneret that is rotating. This leads to formation of a jet flow. This is a process that has been developed and shown experimentally to generate macro- and nano-fiber jets. So far, there has been a number of studies that were either in theoretical and computational or in experimental areas of the mechanics of rotating fiber jet flows at low or high rotation rates (Sarkar *et al.*, 2010; Vazquez *et al.*, 2012; Altecor *et al.*, 2012; Padron *et al.*, 2013; Taghavi and Larson, 2014a,b; Noroozi *et al.*, 2017, 2020; Riahi, 2018a,b, 2020, 2021; Riahi *et al.*, 2018; Riahi and Orizaga, 2022). The studies were needed to understand how to produce fibers for possible use in various applications such as those in defense, energy, aerodynamics and health areas, etc. In the theoretical and computational modeling studies that have been done so far for such jet flows, an essential approach that has been used is based on the consideration that the jet is very thin. Such an approach is called a slender jet approach, and it is meant that the ratio of the fiber jet radius to its centerline scale is fixed to be small as compared to a value of one.

A notable experimental study done during a forcespinning process was due to Padron *et al.* (2011). These authors applied a high speed photography procedure to further insight into the nature of the whole mechanism that was involved in fiber jet formation by the forcespinning process. The authors noted that during the forcespinning process, a polymeric fluid was driven by rotational forces into an orifice that was located in a spinneret rotating and producing rotational forces. That resulted in a jet with a curved centerline moving forward in the three-dimensional space. The authors determined the effects at a high rotation rate of the rotational forces generated by the rotating spinneret. They also determined the effect of polymeric viscosity of the

fluid solution in their experiment, where they tested such an effect by using polymeric fluid solutions having different weight percentage of PEO (Polyethylene oxide) concentration in water. In addition, they determined a projection of the trajectory of the nano-fiber jet in a horizontal plane, speed of the jet and diameter of the nano-fiber jet.

The first investigation of the rotating jet flow generated by centrifugal spinning which developed the so-called regularization approximations were due to Taghavi and Larson (2014a,b). These authors studied a two-dimensional version of the steady jet flow of a Newtonian viscous fluid formed by centrifugal spinning. They introduced an approach referred to as a regularization procedure where the original dynamic equation for momentum of the fluid in the radial direction was strongly modified and changed. The authors introdused an additional term which was a third derivative with respect to the arc length of the curvature of the jet flow. They then determined computationally the solution of their regularized model with prescribed boundary conditions. However, there was no justification from a mathematical fluid mechanics point of view for such changes and modifications of the original fluid dynamical equations in the steady and two-dimensional version. But the authors explained the reasoning for using their regularization approach as numerically divergent and lacking solutions for rotating driven jet quantities. Some authors in the past studies on such rotating jet flow problems at high rotation rates tried using asymptotic techniques. Noroozi *et al.* (2017) investigated a three-dimensional steady rotating polymeric jet at a high rotation rate using and extended the regularization procedure (Taghavi and Larson, 2014a,b). The authors made a strong additional extension to the regularization procedure by, in particular, including third derivatives in the jet arc length of two local curvature functions in the radial component of the momentum equation. The authors then determined the solution to their new regularization model using a collocation method and calculated some jet quantities such as radius of the jet flow.

It should be also noted that the work by Noroozi *et al.* (2020) extended the regularization approach (Taghavi and Larson, 2014a,b) to investigate the steady rotating fiber jet flow of a viscous Newtonian fluid at a large rate of rotation. The authors also took into account the effects due to mass diffusion and an approximated form of the drag force exerted by the ambient air. The authors also performed some experimental work for a fluid solution of a polymeric nature. Regarding their regularization approximations, they notably needed to restrict the applicability of their model by disregarding all higher order terms in their regularization system. This resulted in the validity of their findings only to apply to a very thin interval for the arc length just in the vicinity of the exit section of the fiber jet flow.

Although the emphasis of the present article is mostly on the high rotation regime for the rotating viscoelastic jet. We find useful to briefly state several research investigations that were completed by Riahi and his co-authors (Riahi, 2018a, 2020, 2021; Riahi *et al.*, 2018; Riahi and Orizaga, 2022). In the last several years, even though those studies were at a low rotation rate regime because a number of different aspects were rather similar to those presented in this paper, which include methodology and type of the fiber jet determined based on an experimentally tested variable viscosity formula (Riahi *et al.*, 2018; Riahi, 2020; Riahi and Orizaga, 2022) or viscoelastic type of the jet flow (Riahi, 2018a; Riahi, 2021). However, there are some new aspects of our research on the rotating viscoelastic fiber jet that we included in the present investigation.

In the present paper, we include our newly developed slender body approach where the aspect ratio of radius of the jet at the orifice to the jet centerline scale is assumed to be a considerably small and positive constant ε. We also restrict the jet centerline domain to begin at a location very close to the orifice center but not at a such center in order to avoid possible numerical divergence and singularity there (Taghavi and Larson, 2014a). In addition, in contrast to the previous studies (Riahi, 2018a,b, 2020, 2021; Riahi *et al.*, 2018; Riahi and Orizaga, 2022), we employ proper scaling and perturbation techniques to investigate forcespinning of a three--dimensional nonlinear viscoelastic jet system at high rotation rates, on the basis of full fluid

equations of motion and dynamical laws. We were successfully able to determine macro and nano--fiber jet quantities at high rotation rates. This is the first time that such a proper scaling and perturbation approach, based on firm mathematical and fluid mechanics foundations, is capable for selected values of the parameters in the experimental range to predict macro- and nano-fiber jets at a moderate value of the arc length from the exit section of the jet flow. Our calculated results indicated, in particular, new profiles for the fiber jet radius and other jet quantities, which are notably different from the corresponding ones for low rotation rates (Riahi, 2018a, 2021) or those at high rotation rates determined by the regularization approach (Noroozi *et al.*, 2017, 2020) which involved severe approximations to the fluid mechanics equations for the jet.

2. Mathematical formulation

We show where the rotating viscoelastic jet flow begins by describing the original form of the governing fluid mechanics equations (Riahi, 2021) provided in a coordinate system rotating with the spinneret at the same rotational speed. Such a coordinate frame is attached and totally fixed to the spinneret (Fig. 1) for a forcespinning system (Altecor *et al.*, 2012; Riahi, 2021). In this figure, the Cartesian coordinate (X, Y, Z) system attached to the rotating spinneret is shown. In addition, its angular velocity of rotation is Ω, which is the same as that of the rotating spinneret, and whose axis along the vertical axis opposite to the gravity force $\mathbf{g}$. In addition, o is the spinneret centre and c is a half length of the spinneret. The coordinate of the jet centreline at the jet exit is $X = c$ and $Y = Z = 0$.

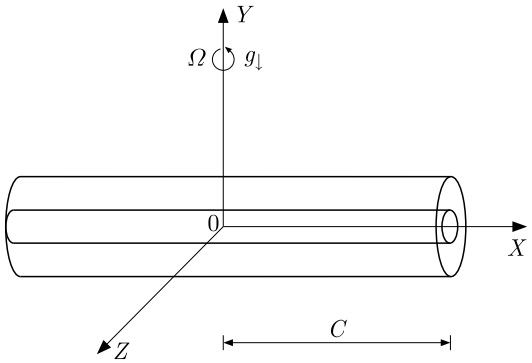

Fig. 1. Coordinate system and spinneret rotating about the vertical axis

We consider the original fluid mechanics equations for the continuity and momentum in the already described rotating frame for the non-Newtonian jet flow for, where we represent the stress tensor $\mathbf{T}$ by the upper convected Maxwell model as it is appropriate for the viscoelastic jet (Riahi, 2018a; Bird *et al.*, 1987; Larson, 1998). These equations were given in (Riahi, 2021), but are recalled below for sake of the readers' satisfaction

$$\begin{aligned}
&\nabla \cdot \mathbf{u} = \mathbf{0}\\
&\frac{\partial \mathbf{u}}{\partial t} + \mathbf{u}\cdot\nabla\mathbf{u} + \frac{1}{\rho}\nabla P - \frac{1}{\rho}\nabla\cdot\mathbf{T} + \boldsymbol{\omega}\times(\boldsymbol{\omega}\times\mathbf{r}) + 2\boldsymbol{\omega}\times\mathbf{u} + \mathbf{g} = \mathbf{0}\\
&\mathbf{T} = \boldsymbol{\tau} + \eta_s(\nabla\mathbf{u} + \nabla\mathbf{u}^{\mathrm{T}})\\
&-\lambda\frac{\partial\boldsymbol{\tau}}{\partial t} - \boldsymbol{\tau} + \lambda(-\mathbf{u}\cdot\nabla\boldsymbol{\tau} + \nabla\mathbf{u}^{\mathrm{T}}\cdot\boldsymbol{\tau} + \boldsymbol{\tau}\cdot\nabla\mathbf{u}) + \eta_p(\nabla\mathbf{u}^{\mathrm{T}} + \nabla\mathbf{u}) = \mathbf{0}
\end{aligned} \tag{2.1}$$

where all the symbols were already defined in (Riahi, 2021), but here we briefly describe them so that the readers have a self-contained article. Here $\mathbf{u}$ is velocity vector of the jet, P is pressure, $\mathbf{T}$ is stress tensor, ρ is density of the fluid, $\mathbf{g}$ is the gravity force per mass unit, t is time variable,

$\boldsymbol{\omega}$ is the angular velocity vector with magnitude Ω (Padron *et al.*, 2013; Riahi *et al.*, 2018), $\mathbf{r}$ is the position vector, η_p and η_s are viscosities of polymer and solvent, respectively, and λ is relaxation time. The cartesian coordinate system (X, Y, Z) is already described and shown in Fig. 1. As in (Riahi, 2021) and in experiments (Padron *et al.*, 2013), the present model is three--dimensional in space and, thus, includes the effect of gravity. The condition for the fiber jet arc length is given below

$$\Big(\frac{\partial \mathbf{X}}{\partial s}\Big)^2 + \Big(\frac{\partial \mathbf{Y}}{\partial s}\Big)^2 + \Big(\frac{\partial \mathbf{Z}}{\partial s}\Big)^2 - 1 = 0 \tag{2.2}$$

Here s is arc length along the centerline of the jet. Thus, $\mathbf{X}$, $\mathbf{Y}$ and $\mathbf{Z}$ are the components of $\mathbf{r}$ of a point on the centerline of the jet with respect to the coordinate (X, Y, Z) system.

Original Eqs. (2.1) and (2.2) are subjected to the known kinematic and dynamic conditions at the boundary of the free surface of the jet flow (Chhabra *et al.*, 2008), which are

$$\begin{aligned} &-\frac{\partial \beta}{\partial t} = \mathbf{u}\cdot\nabla\beta \qquad\qquad \beta \equiv n - R(s,\phi,t) \\ &(\mathbf{T} - P\mathbf{I})\cdot\mathbf{n} + \sigma\kappa\mathbf{n} = \mathbf{0} \end{aligned} \tag{2.3}$$

These boundary conditions are already given in (Riahi *et al.*, 2018; Riahi, 2021), and so here the new symbols are defined briefly. Here, n and ϕ are radial and azimuthal variables, respectively, in a polar coordinate in a plane perpendicular to the jet centerline, $\mathbf{n}$ is a unit normal vector in outward direction to the surface of the jet, $\mathbf{I}$ is the unit matrix, R is radius of the jet, σ is surface tension, and $\kappa \equiv \nabla\cdot\mathbf{n}$ is a double mean curvature of the boundary of the jet. Here (2.3) are given by independent variables (s, n, ϕ) of local orthogonal curvilinear coordinates. We also have the following main boundary conditions at the boundary of the orifice

$$\begin{aligned} &\mathbf{X} = \mathbf{Y} = \mathbf{Z} = \frac{\partial \mathbf{Y}}{\partial s} = \frac{\partial \mathbf{Z}}{\partial s} = \mathbf{0} \qquad\qquad \frac{\partial \mathbf{X}}{\partial s} - 1 = \mathbf{0} \\ &u - U = 0 \qquad\quad 0 = R - r_o \quad \text{at} \quad s = s_1 \end{aligned} \tag{2.4}$$

where r_0 is the orifice surface at the exit section of the fiber jet, U is the centerline velocity at the orifice's boundary and s is taken as the jet centerline from the orifice boundary in order to avoid presence of any singularity that may exist at the orifice center (Taghavi and Larson, 2014a). So, based on the value for $r_o = 1\,\text{mm}$ (Padron *et al.*, 2013) and our selected value for ε, which will be described below, we choose $s_1 = 0.001\,\text{m}$.

Equations (2.1)-(2.4) are then made in a non-dimensional form, and such a procedure is given in (Riahi, 2021). Thus, we describe it briefly here. We use the scaling U for $\mathbf{u} = (u, v, w)$, ρU^2 for pressure, r_0 for n and R, s_0 for s and (X, Y, Z), C/U for t and $(\eta_s + \eta_p)U/r_0$. Here s_0 is the centerline scale for the jet. For simplicity, we present the resulting non-dimensional variables in terms of the same original symbols. The resulting system contains several non-dimensional parameters, which are as follows. Rossby number $\text{Ro} = U/(\Omega s_0)$ is a rotational parameter, Froude number $\text{Fr} = U/\sqrt{s_0 g}$ represents the gravity effect, Weber number $\text{We} = \rho U^2 r_o$ is a surface tension parameter, Reynolds number $\text{Re} = U s_0/(\eta_s + \eta_p)$ represents the viscosity effect, Deborah number $\text{De} = \lambda U/s_0$ is a viscoelastic parameter, $\eta = \eta_p/(\eta_s + \eta_p)$ is the viscosity ratio, and a small aspect ratio is given by $\varepsilon = r_o/s_0$ ($\varepsilon \ll 1$), where λ is the relaxation time.

Typical values of units in the SI system for constants and scales described above have been chosen in the range of values which are in agreement mostly with those in the experimental studies (Padron *et al.*, 2013; Noroozi *et al.*, 2020) and are given as follows. The velocity scale is $U = 0.3\text{-}2.0\,\text{m/s}$, jet radius scale $r_0 = 0.2\text{-}0.3\,\text{mm}$, fluid density $\rho = 1000.0\text{-}1070.0\,\text{kg/m}^3$, surface tension $\sigma = 2.0\text{-}2.5\dot{\text{N}}/\text{m}$, angular velocity $\Omega = 200.0\text{-}2200.0\,\text{rad./s}$, viscosity of the polymer $\eta_p = (1.2\text{-}3.5)(10^{-3})\,\text{Ns/m}^3$, viscosity of the solvent $\eta_s = (0.8\text{-}1.4)(10^{-3})\,\text{Ns/m}^3$, relaxation time $\lambda = (0.001\text{-}100.0)\,\text{s}$, and acceleration due to gravity is $g = 9.81\,\text{m/s}^2$.

We already assumed that the fiber jet is a long and very slender jet, then the aspect ratio ε is a quite small parameter ($\varepsilon \ll 1$), so that we take its value to be $\varepsilon = 0.001/3$. Such a value is chosen for our scaling analysis in order to make sure that our modeling system, which will be determined based on the leading order terms in powers of ε for original Eqs. (2.1)-(2.3), is sufficiently accurate. The scaling analysis is based on the expansions for the dependent variables that are given below

$$\begin{aligned}
&(u, v, w) = [u_0 + \varepsilon n u_1 + \ldots, \varepsilon n v_1 + \ldots, \varepsilon n w_1 + \ldots] \\
&(P, R) = [P_0 + \varepsilon n P_1 + \ldots, R_0 + \varepsilon R_1 + \ldots] \\
&(X, Y, Z) = [X_0 + \varepsilon X_1 + \ldots, Y_0 + \varepsilon Y_1 + \ldots, Z_0 + \varepsilon Z_1 + \ldots] \\
&\tau_{ij} = \tau_{0ij}\delta_{ij} + \varepsilon n \tau_{1ij} + \ldots
\end{aligned} \tag{2.5}$$

where u_i, P_i, R_i, X_i, Y_i, Z_i ($i = 0, 1, \ldots$) and v_i and w_i ($i = 1, 2, \ldots$) are, in general, functions of s, ϕ and t. The subscripts ij for τ_{ij}, which are functions of s and ϕ, in $(2.5)_4$, mean that normal stress components in the directions of s and n are for $i = j = 1, 2$. However, the tangential components of stress are if $i \neq j$. Here, δ equal to 1 for $i = j$ and 0 for $i \neq j$.

Using (2.5) in the system, we apply the small and constant parameter ε to properly scale variables of the system. System (2.1) and (2.2) is then simplified and reduced for the steady case. We retain only the leading order terms and make additional simplifications to arrive at a final simplified and reliable system which is found to be dependent only on u_0, R_0, X_0, Y_0, Z_0 and normal stress terms. Dropping the subscripts for simplicity, the resulting form of the modeling system is given below

$$\begin{aligned}
&u\frac{\partial u}{\partial s} = \frac{1}{\mathrm{We}R^2}\frac{\partial R}{\partial s} - \frac{E_9}{\mathrm{Fr}^2} + \frac{2u}{\mathrm{Ro}}\Big(E_8\frac{\partial Z}{\partial s} - E_{10}\frac{\partial X}{\partial s}\Big) + \frac{1}{\mathrm{Ro}^2}[E_8(X+1) + E_{10}Z] \\
&\quad + \frac{1-\eta}{\mathrm{Re}}\Big(\frac{6}{R}\frac{\partial R}{\partial s}\frac{\partial u}{\partial s} + 2\frac{\partial 2u^2}{\partial s}\Big) + \frac{1}{\mathrm{Re}R^2}\frac{\partial R^2(\tau_{11} - \tau_{22})}{\partial s} \\
&u\frac{\partial R}{\partial s} = -\frac{R}{2}\frac{\partial u}{\partial s} \\
&\Big(\frac{\partial X}{\partial s}\frac{\partial^3 X}{\partial s^3} + \frac{\partial Y}{\partial s}\frac{\partial^3 Y}{\partial s^3} + \frac{\partial Z}{\partial s}\frac{\partial^3 Z}{\partial s^3}\Big)\frac{\partial u}{\partial s} + \frac{2}{3}\frac{\partial E_0}{\partial s} = 0 \\
&\Big(-u^2 + \frac{1}{\mathrm{We}R}\Big)E_0 - \frac{2u}{\mathrm{Ro}}\Big(E_{11}\frac{\partial Z}{\partial s} - E_{13}\frac{\partial X}{\partial s}\Big) + \frac{E_{12}}{\mathrm{Fr}^2} + \frac{1}{\mathrm{Ro}^2}[E_{11}(X+1) - E_{13}Z] \\
&\quad + \frac{1}{\mathrm{Re}}\Big(2\frac{\partial \eta}{\partial s}uE_0 + \frac{7\eta E_0}{3}\frac{\partial u}{\partial s} + \frac{(5\eta u}{3}\frac{\partial E_0}{\partial s}\Big)
\end{aligned} \tag{2.6}$$

and

$$\tau_{11} + \mathrm{De}\Big(u\frac{\partial \tau_{11}}{\partial s} - 2\tau_{11}\frac{\partial u}{\partial s}\Big) = 2\eta\frac{\partial u}{\partial s} \qquad \tau_{22} + \mathrm{De}\Big(u\frac{\partial \tau_{22}}{\partial s} + \tau_{22}\frac{\partial u}{\partial s}\Big) = -\eta\frac{\partial u}{\partial s} \tag{2.7}$$

where the expressions for E_0-E_{13}, which are functions of X, Y and Z, and together with their derivatives with respect to s and are very lengthy, will not be given here. The boundary conditions are

$$\begin{aligned}
&X = Y = Z = \frac{\partial Y}{\partial s} = \frac{\partial Z}{\partial s} = u - 1 = R - 1 = \frac{\partial X}{\partial s} - 1 = 0 \qquad \text{at} \quad s = s_1 \\
&\tau_{11} - 2\eta\frac{\partial u}{\partial s} = \tau_{22} + \frac{\partial u}{\partial s} = 0 \qquad \text{at} \quad s = s_1
\end{aligned} \tag{2.8}$$

The above modeling system of equations and the boundary condition are based on the leading order terms in powers of the aspect ration ε in our scaling and perturbation procedure. Thus, it is important to make sure that higher order terms in our procedure will affect the results based

on our above modeling system, and we can achieve such assurance by keeping the aspect ration ε as small as we think it should. We already provided a very small value for ε that can make higher order terms, which are of the order ε^n $(n \geqslant 2)$, extremely small without any influence on the outcome of our modeling system. Hence, the modeling system based on the proper scaling and perturbation procedure very much relies on the way we adjust the aspect ratio. Even though such an adjustment is not unique, it provides reasonably assurance that the results of the modeling system can be reliable.

The imposed stress conditions at the exit section $s = s_1$ of the jet are chosen to be simply Newtonian since our early results based on numerical testing of our computational outcome indicated that changes of the stress condition were rather insensitive to the final results. This outcome is also consistent with the assumption that the molecules of the polymeric fluid have not been able to be stretched right at the boundary of the orifice.

3. Results and discussions

We present in this Section the results and discuss the solutions to the modeling system of the jet flow given by Eqs. (2.6)-(2.8) found by a computational procedure solving the initial value problem. We first convert Eqs. (2.6) and (2.7) into a system which consists of thirteen first order ordinary differential equations, where the independent variable is the arc length of the jet centerline s. Treating this system as an initial value problem, we solve it using a Runge-Kutta scheme of the fourth order, which is quite efficient (Ascher *et al.*, 1995). Since Eqs. (2.6) and (2.7) contain higher derivatives for some dependent variables, and Eqs. (2.8) does not have enough conditions at $s = s_1$ for solving the above stated 13 equations, we first carry out an asymptotic procedure in the limit of $s \to s_1$, which is similar to that applied before the two-dimensional approximation case where the rotation rate was low (Riahi, 2018) to determine the asymptotic solutions for a very small s $(0 < s \ll 1)$ in Eqs. (2.6) and (2.7). Then, we found the leading order expressions for the dependent variables, which were used to find some needed boundary conditions at $s = s_1$. We determined the solutions for such an initial value problem numerically and generated data for the jet quantities for different parameter values that were chosen to be in the range of experimental studies (Padron *et al.*, 2013; Noroozi *et al.*, 2017) during the forcespinning process. We were also careful that our numerical scheme did not lead to numerical instability by choosing a sufficiently small step size of the adjacent grid point, etc.

We generated computational data for the jet centerline speed, radius of the jet, trajectory of the jet in three-dimensional space, rate of strain, tensile force and rate of stretching for different values of all non-dimensional parameters of our modeling system. As we described before, the values of parameters were chosen to be in the range of those reported by Noroozi *et al.* (2017) in the experiments by Padron *et al.* (2013).

Figure 2 shows the radius R of the fiber jet versus the arc length s of the jet for the Weber number $\mathrm{We} = 0.037$, Reynold number $\mathrm{Re} = 0.2$, Froude number $\mathrm{Fr} = 1.0$, viscosity ratio $\eta = 0.4$ and different values for Deborah number $\mathrm{De} = 0.1,\ 0.05$ and Rossby number $\mathrm{Ro} = 0.059,\ 0.061$. We can observe from this figure that the effects of viscoelasticity and forces due to rotation are destabilizing because the radius of the jet decreases as viscoelasticity and/or rotational effects increase. Such effects of the rotation and viscoelasticity are also seen to be enhanced rapidly as the arc length of the jet increases. The fiber radius can reach macro- and nano-scale values for the jet not too far away from the exit section as we will explicitly explain later in this Section by providing a figure and generated data. The profile for the radius of the jet versus the arc length of its centerline at a such higher rotation rate is found to be very different from the results obtained for the high rotation rate by using the regularization modeling approach (Noroozi *et al.*, 2017, 2020) and for the low rotation rate for the asymptotic procedure (Riahi, 2018b). At the

high rotation rate, the fiber radius rapidly decreases with the increasing arc length for the jet close to its exit section. Such a rate of decrease is enhanced by the increasing Deborah number, while the arc length rate with the increasing s decreases for the jet centerline beyond some distance from the jet exit section. Our present results indicate that in contrast to those reported in (Riahi, 2018b) for low rotation rate cases, the fiber radius decreases as either rotation rate or relaxation time increases at a relatively smaller rate.

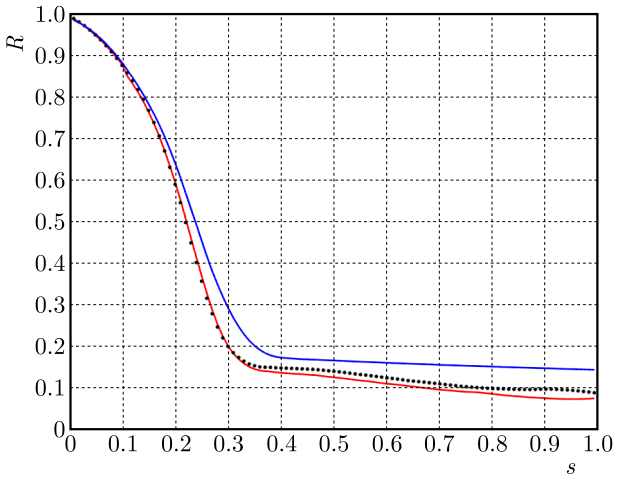

Fig. 2. Radius of the jet R versus arc length s of the jet centerline for the Weber number We = 0.037, Reynolds number Re = 0.2, viscosity ratio $\eta = 0.4$, Froude number Fr = 1.0, Deborah number De = 0.1 and Rossby number Ro = 0.059 (red line); De = 0.1 and Ro = 0.061 (dotted black line) and De = 0.05 and Ro = 0.061 (blue line)

The other noticeable observation in Fig. 2 is that at high rotation rates such as considered in this figure, the jet fiber significantly decreases with a very small increase in the rotation rate, and such rate of decrease is more noticeable for jets not too close to their exit section. An increase in the viscoelastic effect also decreases the jet radius but is less significant as compared to that due to the increase of the rotation rate.

Figure 3 presents the jet speed u versus arc length s for the Weber number We = 0.037, Reynolds number Re = 0.2, Froude number Fr = 1.0, viscosity ratio $\eta = 0.4$, Deborah number De = 0.05, 0.1) and Rossby number Ro = 0.059, 0.061. This figure shows that the value of speed gets higher as the rotation rate or viscoelasticity grows. In addition, the rate of such an increase is further enhanced when the jet moves away from its exit section. It is again apparent that the rotational forces or viscoelasticity tends to make the fiber jet more intensified which we refer to as some sort of destabilization effect exerted by either rotational or viscoelasticity effects on the speed of the fiber jet. However, a notable result shown in this figure is a significant increase of the jet speed with respect to a rather moderate increase in viscoelasticity. The value of the jet speed in also visibly higher for the jet not too close to its exit section. We also made some comparison between the present results at a high rotation rate with the results from the previous studies at a low rotation rate (Riahi, 2020, 2021). It is found that in the present case with high rotational forces, the speed of the jet and its rate of increase with respect to either arc length of the jet centerline, rotation rate or viscoelasticity takes higher values as the rotation rate, viscoelasticity or arc length takes higher values than those in the previous results (Riahi, 2020, 2021) in the case of a small rotation rate. In addition, the present profiles for the fiber jet speed are notably different from the previous results at small rotation rates as well as from those based on the high rotation rate model constructed by the regularization approximation. We can conclude by the combined results provided in Figs. 2 and 3 and our further data that the jets produced at a very high speed are in fact very thin.

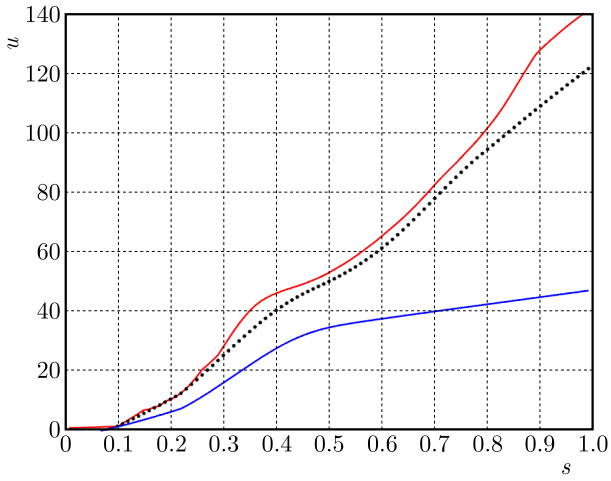

Fig. 3. Jet speed u versus arc length s of the jet centerline for Weber number We = 0.037, Froude number Fr = 1.0, Reynolds number Re = 0.2, viscosity ration $\eta = 0.4$, Deborah number De = 0.1 and Rossby number Ro = 0.059 (red line), De = 0.1 and Ro = 0.061 (dotted black line) and De = 0.05 and Ro = 0.061 (blue line)

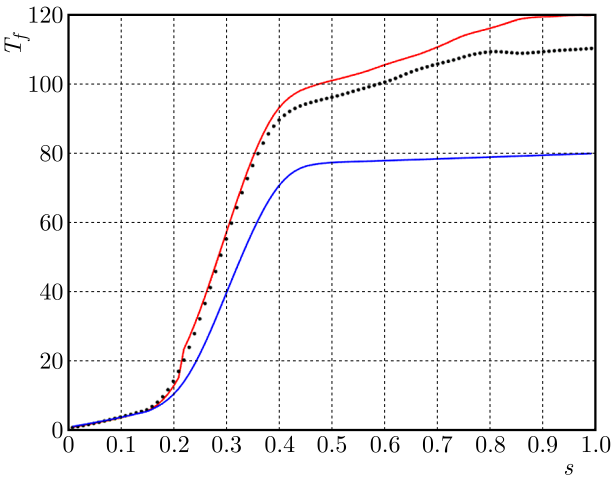

Fig. 4. Tensile force T_f versus arc length s of the jet centerline for the Weber number We = 0.037, Reynolds number Re, viscosity ratio $\eta = 0.4$, Froude number Fr = 1.0, Deborah number De = 0.1, Rossby number Ro = 0.059 (red line), De = 0.1 and Ro = 0.061 (dotted black line), De = 0.05 and Ro = 0.061 (blue line)

Figure 4 presents the tensile force T_f, whose expression is $R^2(\tau_{11} - \tau_{22})$ as provided in (Riahi, 2018a, 2021) versus the arc length s of the jet centerline for Weber number We = 0.037, Froude number Fr = 1.0, viscosity ratio $\eta = 0.4$, Reynolds number Re = 0.2, Deborah number De = 0.1, Rosby number Ro = 0.059 (red line), De = 0.1 and Ro = 0.061 (dotted black line), De = 0.05 and Ro = 0.061. This figure shows that the effect of the tensile force is intensified remarkably as the magnitude of rotational forces or viscoelasticity effects increase when the arc length of the fiber jet moves away further from its original exit section. We also noted that the rate of change of the tensile force with respect to the arc length of the fiber jet centerline takes higher values as the fiber jet moves away shortly from the orifice. Then it appears that the rate of increase drops as the fiber jet moves much further away from its original exit section. The reduction of the effect of relaxation time is observable in the case of the tensile force as it reduces more deeply and becomes very weakly dependent on the wave length of the jet centerline for jet locations not too close to its exit section. We also made calculation for the fiber jet parameters such as radius, etc. for several Weber numbers. In particular, we found that the radius of the fiber decreases

as the surface tension decreases. This result agrees with physical understanding of the surface tension as it generally exerts some stabilizing effect to slows down the fiber jet, which implies thickening of the jet.

Figure 5 provides some typical results in the Cartesian coordinates (X, Y, Z) of the jet trajectory or, equivalently, of the jet centerline in the three-dimensional domain, where X and Z are in the horizontal plane and Y is in the vertical direction for the given values of Reynolds, Weber, Deborah and Rossby numbers as well as the viscosity ratio η listed in the figure caption and for the Froude number Fr = 0.1 and 1.0. From the results shown in this figure, it can be seen that the local curvature of the jet centerline curve as well as its tightness increase as the effect of the gravity force becomes more significant. This result indicates that the force of gravity tends to speed up the fiber jet since the resultant rotational and gravity forces enhance jet effectiveness, and we refer this to as a kind of destabilizing effect exerted by the gravity force. It can also be seen from this figure that the effect of gravity force makes the jet centerline more three-dimensionally, which is expected since resultant force due to rotation and gravity becomes a more three-dimensional domain. In addition, we also calculated the jet centerline for several fixed values of the parameters Re, We, η and Fr but with different values of Ro and De. We observed that the curvature of the jet trajectory tends to locally increase as the rotational forces or viscoelasticity increase.

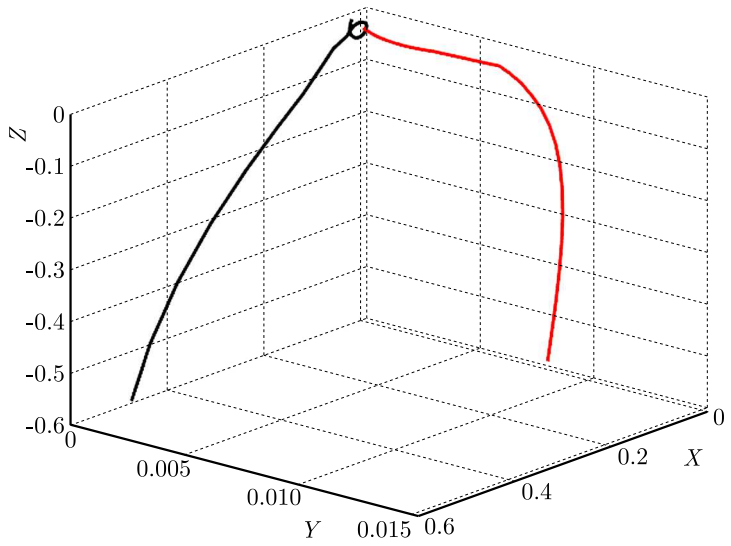

Fig. 5. Jet centerline in terms of the three-dimensional Cartesian coordinate (X, Y, Z) for the Reynolds number Re = 0.1, Weber number We = 0.004, Deborah number De = 0.1, Rossby number Ro = 0.055, viscosity ratio $\eta = 0.4$ and for two values of Froude number Fr = 0.1 (red line) and 1.0 (black line)

Figure 6 provides radius R of the fiber jet versus the arc length s of the jet centerline for Re = 0.2, Ro = 0.06, We = 0.0039, De = 0.1, Fr = 1.0 and viscosity ratio $\eta = 0.4$. We can observe from this figure that the fiber jet radius becomes very small fastly, approaching zero as the fiber jet moves away from its exit section by some rather small distance. The rate of decrease of the jet radius becomes large as the fiber jet moves further away from its exit section. To provide a more explicit demonstration for the fiber jet that reaches a nano-scale level, we also provide in Table 1 some generated data for this figure.

From the experimental studies (Padron *et al.*, 2013; Noroozi *et al.*, 2020), for the production of the polymeric fiber jet we set $r_0 = 0.29\,\text{mm}$ and our already chosen $\varepsilon = 0.001/3$) to make our model sufficiently accurate. The results are given in Table 1. Since both s and R are non-dimensional quantities, we use values given in Table 1 and proceed ih the way we made non--dimensional system in Section 2. We have dimensional arc length $ss_0 = (\varepsilon/r_0)s$, where s_0 is the dimensional scale of the fiber jet and r_0 is the scale for the fiber jet, so dimensional jet radius

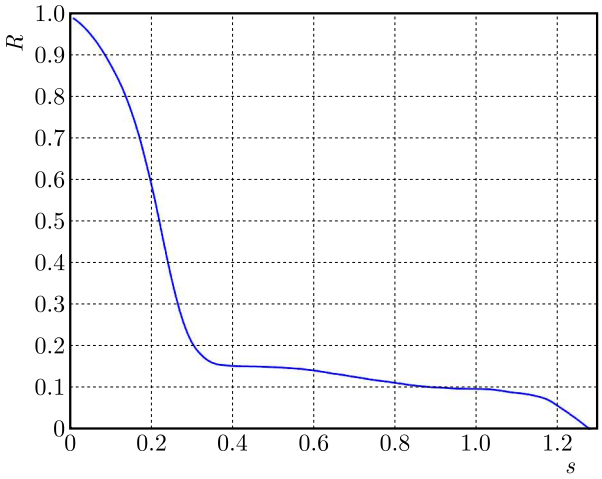

Fig. 6. Radius of the jet R versus the arc length for the jet centerline s for Re = 0.2, Ro = 0.06, We = 0.0039, De = 0.1, Fr = 1.0 and $\eta = 0.4$ with a nano-fiber jet achieved at a moderate distance from the jet exit section

is Rr_0. We now choose a value for the arc length from those listed in Table 1, that is $s = 1.10$, which corresponds to the fiber jet radius $R = 0.0776$. Then we find that the macro-scale jet is achieved at dimensional arc length of about 0.957 m with dimensional fiber radius of about 22.5 μm. Next, we choose from Table 1 $s = 1.30$, which corresponds to $R = 0.0003$. We then find that the nano-fiber jet is reached at dimensional arc length of about 1.131 m with dimensional fiber radius of about 87.0 nm.

Table 1. Generated data for Fig. 6, where s is the arc length of the jet centreline and R is the jet radius

s	0.0	0.2	0.4	0.6	0.8	1.0	1.10	1.20	1.275	1.30
R	1.0	0.591	0.152	0.133	0.108	0.0958	0.0776	0.0539	0.0019	0.0003

In addition to the above results for the radius of the fiber jet, we also calculated additional data for several other fiber jet quantities versus several parameters. We found that as compared to the already determined results for low rotation rates (Riahi, 2020, 2021), the present results at high rotation rates have notably higher speeds of the fiber jet, tensile force, rate of strain and rate of jet stretching. The corresponding arc length increases as the magnitude of rotational forces, viscoelasticity or the arc length of the fiber jet centerline increase.

We now compare the present results that we obtained based on proper scaling and perturbation methods at high rotation rates with the related studies done in the past (Noroozi *et al.*, 2017; Noroozi *et al.*, 2020) for fiber jets at high rotation rates, which are given as follows. Noroozi *et al.* (2017) extended the earlier developed regularization approach (Taghavi and Larson, 2014a,b) to study fiber jets generated by centrifugal spinning. Their extension included a number of additional assumptions and simplifications. They studied a non-Newtonian jet on the basis of a power-law model for the stress tensor, and they calculated the results numerically using a collocation method. Their calculated result for the radius and speed of the jet versus arc length of the jet centerline appeared to merge with the results for the inviscid case and remained as inviscid parameters for the arc length beyond some moderate value. These results qualitatively agree with the present results only for very small values of the arc length of the jet centerline. Noroozi *et al.* (2020) also extended the regularization procedure (Taghavi and Larson, 2014a,b) and studied centrifugal spinning of a Newtonian jet at high values of the rotation rate. The authors also included the presence of mass diffusion and an approximated version of the air-drag force in their jet modeling system. They significantly simplified their

model by discarding all higher order terms, so that their results appeared to become applicable only within the vicinity of the jet orifice. They ignored the presence of gravity by assuming that the rotational forces are much greater than the gravity force, and, in addition, they assumed that the jet centerline is in a fixed horizontal plane. They treated their modeling system as a boundary value problem and solved it numerically. Their graphical result for the fiber radius variation versus arc length was found to have some qualitative similarity with the present result only for sufficiently small values of the arc length. From the point of view of applied mathematics and fluid mechanics, we should note that a comparison between our present results presented in details in Section 3 and the results by Noroozi *et al.* (2017, 2020) indicated that our new findings are based on proper scaling. Our modeling system was based on original fluid mechanics laws and equations as well as perturbation technique, whereas the other related studies (Noroozi *et al.*, 2017, 2020) were basically based on the regularization approach, neglecting the gravity force and focusing mostly on a two-dimensional version of the fiber jet. Our present results take into account three-dimensionality of the jet in the presence of gravity force at high rotation rates, and we implemented a new slender body approach and a procedure to avoid the presence of numerical divergence. Our results predicted new fiber jet profiles for different jet quantities, and we were able to predict macro and nano-fiber jets at particular locations of the fiber jet at a moderate distance from the orifice.

4. Conclusions

We have considered a mathematical model describing the interesting and yet complicated dynamics of a thinning jet due to a rotating mechanism (forcespinning). We have presented simplifying assumptions and modeling conditions that are useful to treat such a complicated system of equations, and we believe that this approach provides a good point of reference fof such s problem. In this paper, we developed a theory based on full fluid mechanics laws and equations providing a model for a nonlinear three-dimensional viscoelastic jet system with the gravity force. It enables using of the upper convected Maxwell constitutive equations for the viscoelastic stress tensor in the momentum equations during the forcespinning process at high rotation rates. We applied a slender body assumption for the jet flow that started at a location very close to the orifice center and kept a sufficiently small value of the jet aspect ratio to maintain an accurate modeling system formed on the basis of the leading order terms in powers of a very small jet aspect ratio and with proper scaling of the jet variables. We determined numerically macro- and nano-fiber jet solutions for the modeling system. Our results for high rotation rates came from our newly developed model that for the first time predicted macro- and nano-fiber jets at a moderate distance from the jet initial formation. The results of our model were in contrast to the results found by regularization approximations (Noroozi *et al.*, 2017, 2020). The values of the fiber jet quantities and their rates of changes with respect to the arc length and parameters were found to be quite different from the corresponding ones from the regularization procedure at high rotation rates. We observed that the jet speed, stretching rate, strain rate, tensile force and jet curvature as well as their rates of increase with respect to the arc length of jet centerline were notably raised-up with the growing resultant rotational and gravity force, arc length and viscoelasticity after the jet moved away by a very small distance from the orifice. However, the jet radius and its rate of change with respect to the arc length were reduced significantly with the increasing arc length, resultant rotational and gravity force, viscoelasticity, and the jet radius reached a macro- and nano-scale size after some moderate distance from the jet exit section. The curvature of the fiber jet centerline was found to increase with the growing resultant rotational and gravity force, viscoelasticity and with the decreasing surface tension and the polymer

viscosity. Our overall results indicated that the fiber jet of a non-Newtonian fluid at a very high speed was very thin at the nano-scale level and was experienced by a strong tensile force.

Although the experimental observation of the nano-fiber formation at a high rotation rate have so far indicated that the nano-fiber jet began to form at a considerable time after jet initiation from the orifice. This actually means that after some considerable distance from the jet exit section, our predicted results showing that the initial location of the nano-fiber jet can not be far from the jet exit section opens two possible observations that are given as follows. Firstly, our result was based on particular and selected values of the jet parameters which were within the range from available experiments (Padron *et al.*, 2013; Noroozi *et al.*, 2017, 2020). This can stimulate new experimental efforts by searching selected parameters to determine if nano-fibers can be formed at a distance not far from the orifice, which, if so, it can agree with the present results and can be very valuable in fiber manufzcturing technologies to improve nano-fiber production of high yield. Secondly, an actual fiber jet system in the experiments contains other components that affect jet formation finalizing nano-fiber production, which include stabilizing effects of the ambient drag force, evaporation process of the solvent, temperature and humidity of the environment and the effect of presence of the collection device that collects the fiber. The authors plan to carry out such an additional work for a more completed model in the future, which may improve the present introductory model.

Finally, it should be noted that the present new theory and model for prediction of a nano--fiber scale jet at a moderate distance from the orifice, where computation is based on a rather simple numerical code, indicate that a future simulation of such a model incorporating a more sophisticated code could possibly lead to prediction of sub-nano fiber jets, which can bring a wide range of new ideas and exploration to develop new technologies with tremendous amount of benefits to the advancement of various factors for humanity.

Acknowledgments

S.O. thanks Anwar and Elizabeth from NMT for their continued support. The authors also thank the reviewers' comments and suggestions for an earlier version of this work that improved the quality of the present paper. In addition, S.O. thanks Cristina Villalobos, Timothy Huber and Elda Leal for the office space and hospitality at the University of Texas Rio Grande Valley (UTRGV).

References

1. Altecor A., Mao Y., Lozano K., 2012, Large-scale synthesis of tin-doped indium oxide nanofibers using water as solvent, *Functional Materials Letters*, **5**, 1250020
2. Ascher U.M., Mathheij R.M.M., Russell R.D., 1995, *Numerical Solution of Boundary Value Problems for Ordinary Differential Equations*, Philadelphia, PA, USA: SIAM Publication
3. Bird R.B., Curtiss C.F., Armstrong R.C., Hassager O., 1987, *Dynamics of Polymeric Liquids, vol. 1, Fluid Mechanics*, Wiley, New York
4. Chhabra R.P., Richardson J.F., 2008, *Non-Newtonian Flow and Applied Rheology*, 2nd Ed., Oxford, UK: Butterworth-Heinemann
5. Larson R.G., 1998, *The Structure and Rheology of Complex Fluids*, UK: Oxford
6. Noroozi S., Alamdari H., Arne W., Larson R.G., Taghavi S.M., 2017, Regularized string model for nanofibre formation in centrifugal spinning methods, *Journal of Fluid Mechanics*, **822**, 202-234
7. Noroozi S., Arne W., Larson R.G., Taghavi S.M., 2020, A comprehensive mathematical model for nanofibre formation in centrifugal spinning methods, *Journal of Fluid Mechanics*, **892**, A26-48

8. Padron S., Caruntu I.D., Lozano K., 2011, On 2d forcespinning modeling, *Proceedings of the 2011 ASME International Mechanical Engineering Congress and Exposition*, IMECE2011-64823, USA: ASME Publications, 821-830

9. Padron S., Fuentes A., Caruntu D., Lozano K., 2013, Experimental study of nanofiber production through forcespinning, *Journal of Applied Physics*, **113**, 024318

10. Riahi D.N., 2018a, Nonlinear rotating viscoelastic jets during forcespinning process, *Proceedings of the Royal Society, A: Mathematical, Physical and Engineering Science*, **474**, 20180346

11. Riahi D.N., 2018b, Rotating fiber jets during forcespinning with aerodynamic effect, *Journal of Engineering Mechanics*, **144**, 8, 04018069

12. Riahi D.N., 2020, On three-dimensional rotating polymeric fiber jets with gravity effect, *Fluid Dynamic Research*, **52**, 1-18

13. Riahi D.N., 2021, On forcespinning of nonlinear rotating jets of viscoelastic Boger fluids, *Journal of Non-Newtonian Fluid Mechanics*, **287**, 104442

14. Riahi D.N., Lozano K., Cremar L., Fuentes A., 2018, On nonlinear rotating polymeric jets during forcespinning process, *Fluid Dynamics Research*, **50**, 065507

15. Riahi D.N., Orizaga S., 2022, On rotationally driven nonlinear inclined polymeric jet with gravity effect, *Mathematics in Engineering*, **4**, 2, 1-18

16. Sarkar K., Gomez C., Zambrano S., Ramirez M., de Hoyos E., Vasquez H., Lozano K., 2010, Electrospinning to forcespinning, *Materials Today*, **13**, 11, 12-14

17. Taghavi S.M., Larson R.G., 2014a, Regularized thin-fiber model for nanofiber formation by centrifugal spinning, *Physical Review E*, **89**, 023011

18. Taghavi S.M., Larson R.G., 2014b, Erratum: Regularized thin-fiber model for nanofiber formation by centrifugal spinning, *Physical Review E*, **89**, 059903(E)

19. Vazquez B., Vasquez H., Lozano K., 2012, Preparation and characterization of polyvinylidene fluoride nanofibrous membranes by forcespinning, *Polymer Engineering and Science*, **52**, 2260-2265

Manuscript received October 22, 2022; accepted for print January 31, 2023